

Modeling Plain Vacuum Drying by Considering a Dynamic Capillary Pressure

S. Sandoval-Torres,* J. Rodríguez-Ramírez, and L. L. Méndez-Lagunas

Instituto Politécnico Nacional, CIIDIR-Oaxaca, Hornos No. 1003,
Col. Noche Buena, Santa Cruz Xoxocotlan, Oaxaca, Mexico

Original scientific paper
Received: August 17, 2010
Accepted: August 15, 2011

A coupled drying model for wood is proposed by introducing a dynamic capillary pressure. The pressures of non-wetting phase, the wetting phase, and the capillary pressure at equilibrium has been considered as non-static; this approach includes a two-scale model. According to numerical results, liquid, water vapor and air dynamics in the chamber have strong interactions with re-homogenization in the surface, controlled by capillary forces. The results at 60–100 bar and 70 °C are discussed. The phenomenological one-dimensional drying model is solved by using the COMSOL's coefficient form and a global equation format. A good description of drying kinetics, moisture redistribution, and mass fluxes is obtained. A comprehensible transition at the fiber saturation point is well simulated.

Key words:

Wood, vacuum drying, dynamic capillary pressure, COMSOL®

Introduction

Drying is a ubiquitous natural process. The dominant stress during evacuation of free water in wood is the capillary pressure from the tiny menisci.¹ Capillary pressure is normally written as $\Delta p = 2\sigma\cos\theta/r$. In porous media, every meniscus acts like a low-pressure pump trying to suck liquid from other places. Because of the heterogeneity of the pore sizes, the menisci in small pores can produce lower pressure and draw liquid from menisci in large pores. This flow would move the air-liquid interface rapidly through the large pores, creating bursts (Fig. 1).

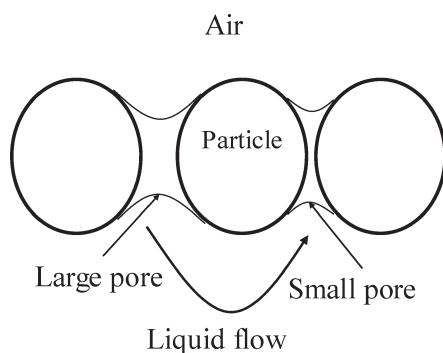


Fig. 1 – Capillary pressure and flow displacement

The bursting process will terminate either when all the pores are small enough to balance the capillary pressure or when the displaced liquid flows to the nearby menisci and reduces the static capillary pressure.

According to Lehmann *et al.*,² drying of wet porous media is an immiscible displacement process of liquid phase by invading gas; hence principles of invasion percolation in gas phase.

The drying kinetics of a porous medium is classically described in three main periods, which depend on the interplay between the external and internal mass transfers during evaporation. The first period is described as a heating up period depending on the external mass transfer; the second period is described as a constant rate period, whereas the third period is identified as a falling rate period dominated by the internal mass transfer.³

In most traditional treatments of capillary pressure, it is defined as the difference between pressures of phases, in this case, air/water vapor and liquid water, and it is assumed a function of saturation. On one hand, recent theories have indicated that capillary pressure should be given a more general thermodynamic definition, and its functional dependence should be generalized to include dynamic effects.⁴ On the other hand, Beserer and Hilfer⁵ affirm that experimental features between capillary pressure and saturations cannot be predicted, since the theoretical derivation of the equations from the well-known laws of hydrodynamics has not yet been accomplished.

Surface areas and surface tensions known to control capillary action and wetting properties do not appear in the mathematical formulation of the traditional theory:

$$v = -\frac{k_r}{\mu}(\nabla p - \rho \cdot g) \quad (1)$$

*Email: ssandovalt@ipn.mx

To generalize Darcy's law to multiphase systems one must assume that the flow of either fluid is hydrodynamically independent of the other fluids. The so-called relative permeability $k_{r\alpha}$ account for the fact that the flow medium and its permeability for each fluid phase α is altered by the presence of all other phases. Based on this idea, Darcy's law is generalized to the velocity field v of each phase α giving:

$$v = -\frac{k_r \cdot k}{\mu} (\nabla p_\alpha - \rho \cdot g) \quad (2)$$

In most applications, the relative permeabilities are treated as functions of saturation $k_\infty = f(S_\infty)$.⁶ But in practice, these relationships are more complicated because of the dependence on physical quantities like surface tensions, contact angles, viscosities, mass densities, pore structure, and the flow conditions have to be considered. Relative permeability is known to be affected by the flow velocity (or pressure gradient) at which the measurements are carried out. Mathematically, relative permeability is also affected by the boundary conditions.⁷ Capillary pressure–saturation and relative permeability–saturation relationships are highly nonlinear, and their determination is often a very difficult task. In this work, we are interested in including a dynamic capillary pressure in a two-scale vacuum drying model. Our study reveals the flow pattern of drying which may ultimately afford a means to control drying in porous media. A deep understanding of drying may provide more fundamentals to determine moisture transport and distribution in porous media.

Mathematical model

In particular, the reader must be aware that all variables are averaged over the REV (Representative Elementary Volume),⁸ hence the expression "macroscopic". This assumes the existence of such a representative volume, large enough for the averaged quantities to be defined and small enough to avoid variations due to macroscopic gradients and non-equilibrium configurations at the microscopic level. The approach proposed by Whitaker⁹ and Perré¹⁰ was followed in this work. The physical model is based on heat, mass and momentum transport at Darcy's scale as obtained by volume averaging the corresponding pore scale balance equations. The average value of variable φ is defined as:

$$\langle \varphi \rangle = \frac{1}{V_{REV}} \int_{REV} \varphi dV \quad (3)$$

In our equations, instead of measuring p_c and S at given equilibrium distributions of the phases, they are determined continuously over time as the flow occurs. This leads to non-uniqueness in the relation between capillary pressure and saturation. On the pore scale, the dynamic contact angle is often given as one reason for the dynamic effect in capillary pressure. The contact angle decreases with increasing flow velocity for drainage and increases with increasing velocity.

Assumptions

We established these considerations:

- Gravitational effects are negligible
- Temperature and pressure in the dryer are homogeneous
- The gas phase is water vapor, which behaves as an ideal gas.
- The bound water has physical properties similar to those of free water.
- Thermodynamic equilibrium, so average temperatures for each phase are the same, and partial vapor pressure is at equilibrium.
- Lack of heat and mass losses assuming ideal isolation.

Then, we can write:

$$\begin{aligned} \bar{T}_v &= \bar{T}_l = \bar{T} && \text{Thermodynamic equilibrium} \\ p_v &= a_w \cdot p_v^{sat} && \text{Vapor pressure} \end{aligned}$$

Compressibility effects in the liquid phase were neglected, meaning $\rho_l^l = \rho_l = cste$ and the gas phase was considered as an air/water vapor ideal mixture.

Mass transport

$$\bar{\rho}_i^g = \frac{m_i \bar{p}_i^g}{RT} \quad (4)$$

$$\bar{p}_g^g = \bar{p}_a^g + \bar{p}_v^g \quad (5)$$

$$\bar{\rho}_g^g = \bar{\rho}_a^g + \bar{\rho}_v^g \quad (6)$$

Pour $i = a$ (air) or v (vapor)

Free water transport is explained by Darcy's law. The velocities of the gaseous and liquid phases are respectively, expressed using the generalized Darcy's law, but as mentioned, gravitational effects are neglected:

$$\bar{V}_l = -\frac{k \cdot k_{rl}}{\mu_l} (\nabla \bar{p}_l^l - \rho_l \cdot g) \quad (7)$$

$$\bar{V}_g = -\frac{k \cdot k_{rg}}{\mu_g} (\nabla \bar{p}_g^g - \rho_g \cdot g) \quad (8)$$

Capillary pressure

Traditionally, one assumes that this relationship is determined under quasi-static or steady state conditions but can be applied to any transient flow processes. The relationship between capillary pressure and saturation might not be unique. Traditionally, $p_c(S)$ is determined under quasi-static or steady state conditions. We have implemented a model by integrating a non-equilibrium capillary pressure. The equilibrium capillary pressure is determined under quasi-static or steady state coefficient. Under transient conditions, the dynamic capillary pressure p_c^{dyn} prevails resulting in a dynamics relationship $p_c^{dyn}(S)$, so mathematically we have:

$$p_{mw} - p_w = p_c = f(S) \quad (9)$$

$$p_{mw} - p_w - p_c^{eq}(S) = -\tau \frac{\partial S}{\partial t} \quad (10)$$

$$p_{mw} - p_w = p_c^{dyn} = -\tau \frac{\partial S}{\partial t} + p_c^{eq}(S) \quad (11)$$

$$p_c = 56.75 \cdot 10^3 (1 - S) \exp\left(\frac{1.062}{S}\right) \quad (12)$$

Where:

$$\tau = \frac{\alpha \cdot \phi \cdot \mu_w}{\lambda \cdot K} \left(\frac{p_d}{\rho_w \cdot g} \right)^2 \quad (13)$$

τ factor is a phenomenological coefficient that takes positive values and depends on water saturation:

$$\tau(S) = \left| \frac{dp_c^{static}}{dS} \right| \tau_B(S) \quad (14)$$

For the relative permeability, we write:

$$k_{rl} = S^2 \quad (15)$$

$$k_{rg} = (1 - S)^2 \quad (16)$$

For the flux of bound water:

$$\begin{aligned} \bar{\rho}_l \bar{V}_l &= \rho_l \frac{k \cdot k_{rl}}{\mu_l} \cdot \nabla p_c - \\ &- \rho_l \frac{k \cdot k_{rl}}{\mu_l} \cdot (\nabla \bar{p}_g^g - \rho_l \cdot g) \end{aligned} \quad (17)$$

For the transport of the vapor phase, we use the ‘‘Dusty gas model’’; this expression considers that vapor water and air mobility depends on pressure and concentration gradient of the gaseous phase:

$$\bar{\rho}_v \bar{V}_v = \bar{\rho}_v^g \frac{k_{eq} \cdot k_{rg}}{\mu_g} \cdot \nabla p_g^g - \bar{\rho}_v^g D_{eq} \cdot \nabla C \quad (18)$$

$$\bar{\rho}_a \bar{V}_a = \bar{\rho}_a^g \frac{k_{eq} \cdot k_{rg}}{\mu_g} \cdot \nabla \bar{p}_g^g - \bar{\rho}_a^g D_{eq} \cdot \nabla C \quad (19)$$

With these parameters, the perturbations in the convective and diffusive dusty transport are considered. The diffusion-sorption model described the bound water migration. A phenomenological approach can explain water flows to the form discussed extensively in literature:

$$J_b = -\rho_s \cdot D_b \cdot \nabla W_b \quad (20)$$

Below FSP, the moisture is considered bound to the cell wall and, therefore, bound water diffusion can be considered the predominant mass transfer mechanism.

Hygroscopic equilibrium

The mass fraction of water vapor C is defined as:

$$C = \frac{\text{vapour mass}}{\text{humid air}} \quad (21)$$

The equilibrium moisture content is expressed by

$$W_{eq} = W(T, aw) \quad (22)$$

$$aw = HR \quad (23)$$

Now we can write macroscopic balances for mass:

For the air mass and water vapor:

$$\frac{\partial \bar{\rho}_a}{\partial t} + \nabla \cdot (\bar{\rho}_a \bar{V}_a) = 0 \quad (24)$$

$$\frac{\partial W}{\partial t} + \nabla \cdot \left\{ \frac{1}{\rho_s} (\rho_l \bar{V}_l + \bar{\rho}_v^g \bar{V}_l + J_b) \right\} = 0 \quad (25)$$

An energy balance allows us to write:

$$\begin{aligned} &\overline{\rho C p} \frac{\partial \bar{T}}{\partial t} + \\ &+ [(\rho_l \bar{V}_l C p_l + J_b C p_l + \bar{\rho}_a^g \bar{V}_a C p_a + \bar{\rho}_v^g \bar{V}_v C p_v)] \nabla \bar{T} - \\ &- (\overline{\rho_b \bar{V}_b} \cdot \nabla h_b) + (h_v K) + (h_v + h_b) K_b - \nabla \cdot (\underline{\lambda} \cdot \nabla \bar{T}) = 0 \end{aligned} \quad (26)$$

The specific heat of wood, expressed by:

$$\overline{\rho C p} = \bar{\rho}_s C p_s + (\bar{\rho}_l + \bar{\rho}_b) C p_l + \bar{\rho}_v C p_v + \bar{\rho}_a C p_a \quad (27)$$

Equation for the mass balance in the dryer

The conservation equations in the dryer chamber are:

$$\frac{d\rho_a^{ch}}{dt} = -\rho_a^{ch} \frac{q_{pump}}{V_{ch}} + \rho_a^{atm} \frac{q_{leak}}{V_{ch}} \quad (28)$$

For the dry-air

$$\frac{d\rho_v^{ch}}{dt} = -\rho_v^{ch} \frac{q_{pump} + q_{cond}}{V_{ch}} + \rho_v^{atm} \frac{q_{leak}}{V_{ch}} + F_m \frac{A}{V_{ch}} \quad (29)$$

Boundary conditions

During drying, the pressure on the surfaces is in equilibrium with the chamber pressure p_{ch} . Recalling that one of the primary variables is the averaged air density, a Dirichlet boundary condition is imposed for the air mass flux. The Dirichlet boundary condition has been modified to form an appropriate non-linear equation for this primary variable. For moisture fluxes, equilibrium between water vapor at surface and the vapor pressure in the chamber was established. About dryer chamber, a mixture water-vapor/dry-air was considered. This mixture depends on dryer (chamber) temperature. With respect to energy fluxes, temperature at the surface is in equilibrium with the chamber temperature. Then, boundary conditions are written as:

$$p_a^g = p_a^{ch} \quad \text{For dry air} \quad (30)$$

$$F_w \cdot \mathbf{n} = h \cdot (\rho_v^g - \rho_v^{dryer}) \quad \text{For water vapor} \quad (31)$$

$$T_{chamber} \approx T_{surf} \quad \text{For energy} \quad (32) \\ \text{[plain vacuum drying]}$$

Materials

Samples of European oakwood belonging to the Fagaceae family were cut from a freshly felled 100-year-old *Quercus pedunculata* tree from a forest in Pessac-Toctoucau, in France. The selected log had a central pith and normal growth ring pattern and there was no apparent compression wood present identified by colour. The experimental setup is a vacuum chamber where pressure is regulated between two values (p_{min} , p_{max}). The chamber was built in glass; one balance is kept inside the chamber in order to log the mass variation of the sample. A thermometer gives the dryer temperature. The heating source is an electrical resistance which temperature is controlled with the help of a PID controller. Experiments are performed on Oakwood disks (7 cm diameter and 2.5 cm height). We call

this drying method “plain vacuum drying” since we do not use a fluid as a drying agent, so only the pump aspiration accelerates mass flux. Pressure in the chamber is controlled at 60–100 mbar. Temperature inside the wood sample is obtained at two different positions. More details are published in Sandoval *et al.*¹¹ The parameters considered in this study are limited by practical implications. The drying temperature should be lower than 80 °C to avoid degradation of wood.

Fig. 2 shows the geometry considered in our equations system 1D. Heat source is an aluminum plate; such plate is heated by an electrical resistance.

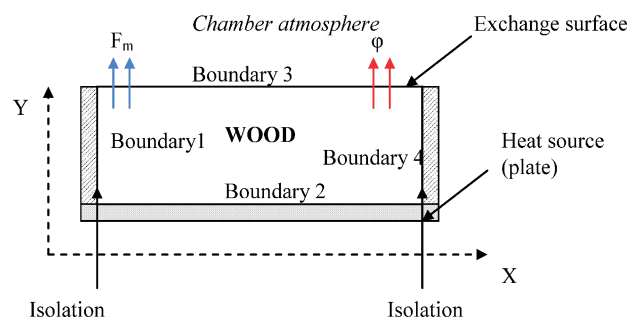


Fig. 2 – Adopted configuration to model vacuum drying

Results and discussion

To solve the equations, the commercial solver COMSOL Multiphysics^{©13} was used. The partial differential equations (material scale) were written in the general form and by using an unsymmetric-pattern multifrontal method. The two ordinary differential equations (dryer scale) were introduced by considering a pump aspiration of $0.0027 \text{ m}^3 \text{ s}^{-1}$ (the real situation). To add a space-independent equation such as an ODE, a Global equation format was chosen. As the time derivative of a state variable (density of air and water vapor) appears, the state variable needs an initial condition; for this reason the initial condition for pressure was the atmospheric pressure. For solving time-dependent variables, the backward differentiation formula (BDF) was applied. The discretization of the time-dependent PDE variables is:

$$0 = L(U, U, U, t) - N_F(U, t) \cdot \Lambda \quad (33)$$

$$0 = M(U, t) \quad (34)$$

This is often referred to as the method of lines. Before solving this system, the algorithm eliminates the Lagrange multipliers Λ . If the constraints $0 = M$ are linear and time independent and if the constraint force Jacobian N_F is constant then the algorithm

also eliminates the constraints from the system. Otherwise, it keeps the constraints, leading to a differential-algebraic system.

The boundary conditions link variables at dryer scale (air and vapor in the chamber) and variables at material scale (mass of air, moisture content, energy). The general form provides a computational framework specialized for highly nonlinear problems. Direct solvers for sparse matrices involve much more complicated algorithms than for dense matrices. The main complication is due to the need for efficient handling of the fill-in in the factors L and U. In COMSOL®, a typical sparse solver consists of four distinct steps:

1. An ordering step that reorders the rows and columns such that the factors suffer little fill, or that the matrix has special structure such as block triangular form.

2. A symbolic factorization that determines the nonzero structures of the factors and creates suitable data structures for the factors.

3. Numerical factorization that computes the L and U factors.

4. A solve step that performs forward and back substitution using the factors. For the most general unsymmetric systems, the solver may combine steps 2 and 3 (e.g. SuperLU) or even combine steps 1, 2 and 3 (e.g. UMFPACK) so that the numerical values also play a role in determining the elimination order. The direct (UMFPACK) solver was used in this simulation.

As we have indicated, the solid phase was considered as rigid and the intrinsic permeability k constant. We have solved this problem in 1D.

Fig. 3 compares predicted and experimental average moisture content in wood. These results correspond to the vacuum drying at 70 °C and 60–100 mbar of pressure. It can be observed that the model is able to predict correctly the average drying kinetic over the 26 hours of this experiment. Theoretical drying kinetics shows good agreement with experimental data. Differences between experimental and simulated kinetics can be explained by a variation of values in permeability, static capillary pressure and transfer coefficients of water vapor, since they can vary from one sample to another. Fluctuations in mass measurements during the initial heating period can be explained by local internal moisture variations within the sample. In the same figure, one can see a good transition between capillary phase and hygroscopic phase (at approximately 0.4 of moisture content). The same figure depicts the chamber pressure. When the vacuum pump starts, an internal pressure reduction is observed. The simulated pressure in the chamber is compared with experimental measures. Comparison

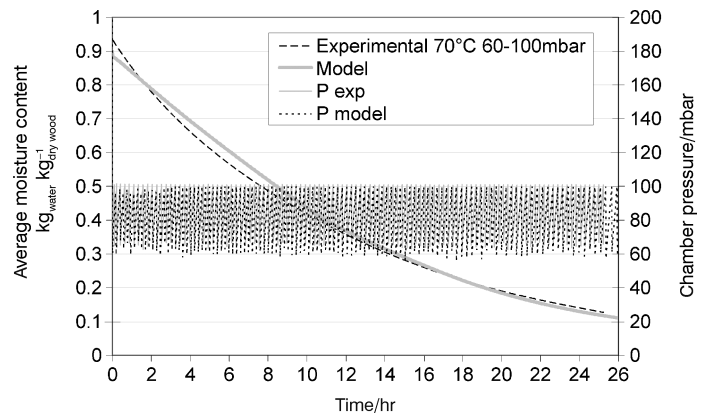


Fig. 3 – Simulation. Vacuum drying kinetics and moisture content in the wood surface.

provides a good confidence of equations and model at lab scale (dryer). Two regimes exist during vacuum drying; the first one is called the active regime, and the second one the passive regime. Model describes both active (pump aspiration) and passive regimes (stopping the aspiration). During vacuum drying, pressure is controlled between two values: p_{\max} and p_{\min} , this fact allows us to obtain a zigzag behavior in chamber pressure that is well represented by simulation.

The moisture movement depends on the permeability of the wood and the internal pressure gradient. The permeability of wood is a dominant factor in controlling moisture movement because the mechanism of moisture movement in wood is flow of water vapor through the cellular structure of wood driven by the pressure gradient in the vacuum drying at a temperature exceeding the boiling point of water (at 60 and 100 mbar the boiling point of water is 35.9 and 45.3 °C respectively). Of course, intrinsic anatomical structures, content of extractives and specific gravity of wood have an influence in permeability.

It is generally admitted that drying time decreases as temperature increase. In this paper, we consider one temperature to facilitate the discussion. During the first regime, acceleration of mass flux is due to pump action, whereas during the second period re-homogenization is due to the pump stopping. A strong coupling between equations at lab scale and material scale exists. This coupling is well-simulated by COMSOL by introducing the boundary conditions. The link between the two scales evolves according to the chamber conditions through the boundary conditions imposed at the surface of the porous medium (large-scale to macroscale) and by the total heat, vapor, air, and, eventually, liquid fluxes leaving the wood surface. A strong effect of the change of the external pressure on internal transfer is when, for instance, a liq-

uid flow is driven by the internal overpressure (high-temperature configuration). The macroscale model must be able to capture such a coupling and, in turn, supply the chamber model with relevant values of the different fluxes leaving the board.

The drying regimes produce natural oscillations at the surface temperature, since during active phase (pump aspiration) a shut of temperature exists due to evaporation, and during the passive phase re-homogenization is developed due to equilibrium. The mass flow is more important during the vacuum pumping, so there is a drop in pressure in the enclosure and consequently faster evaporation on the surface of wood. Evaporation causes an increase in the pressure chamber and a homogenization of quantities in the material. This fact is visible on the flux on the surface. For better explanation, in Fig. 4 we show the average moisture content and moisture distribution at the surface. We can observe a drop in the moisture content around the fiber saturation point (fsp), which indicates that free water has been eliminated. After this point (fsp), the mechanisms of mass transport are mainly due to diffusion, since the moisture evacuated in gaseous phase is more slow. Our proposed model describes physically this transition (Fig. 4). A mass flux is improved during vacuum drying, since the external vacuum reduces the required temperature for evaporation.

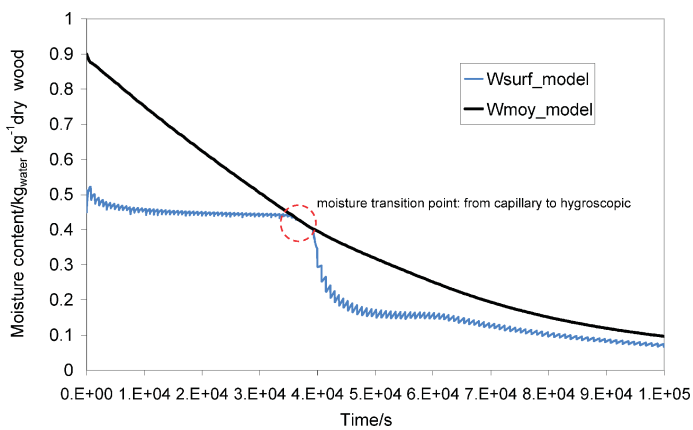


Fig. 4 – Average moisture content and moisture distribution at the surface

In order to estimate the error or deviation of our model, the quadratic error was computed between experimental and numerical data, according to:

$$S = \left[\frac{W_{exp} - W_{model}}{W_{exp}} \right]^2 \quad (35)$$

Fig. 5 depicts these values. It should be observed that at 6 hours of drying and at the end, the

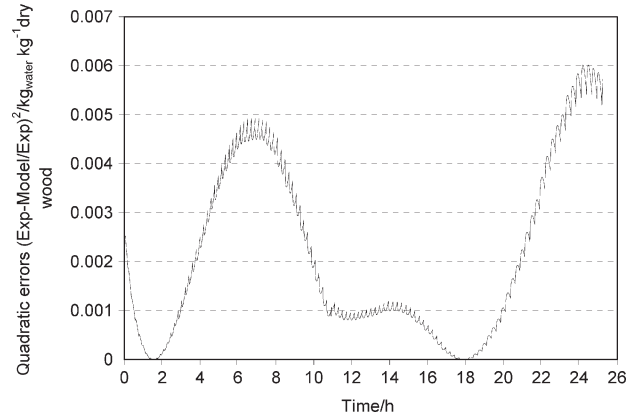


Fig. 5 – Quadratic errors of the simulated drying kinetic

more important deviations are more visible. These deviations are explained by the capillary pressure and permeability function, and by the changes in moisture equilibrium respectively, because the desorption isotherms could change due to biological variations and chemistry (extractives) in wood.

During drying, the wood surface is constantly fed in moisture, but free water is easier to evacuate. The evaporation rate depends mainly on the level of pressure and temperature. By consequence, a more important concentration of water vapor exists in the chamber during this capillary stage, nevertheless global pressure (vapor + air) is regulated between p_{max} and p_{min} . At the very beginning of the process, the chamber pressure equals the atmospheric pressure and the gas mixture consists mainly of air.

Fig. 6 displays the moisture profiles in wood during vacuum drying; this figure displays moisture distribution in the sample. Free water transport is well identified. Two different distributions are visible: the first one explained by capillary forces, and the second by diffusional mechanisms. In the hy-

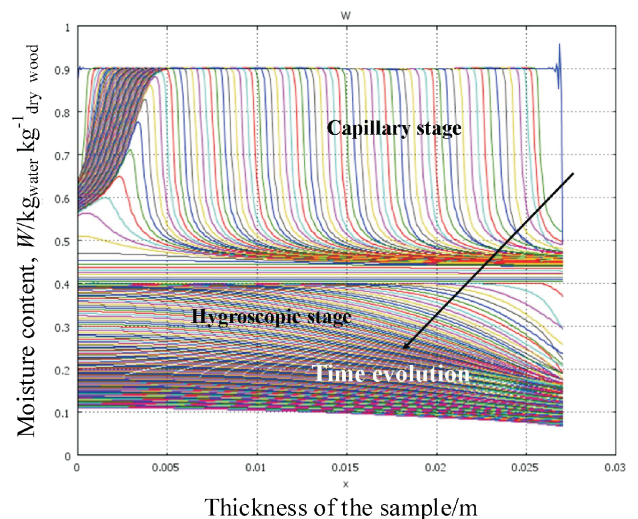


Fig. 6 – Moisture profiles during plain vacuum drying

groscopic stage, the thermodynamic equilibrium between gas phase and bound water allows a less important drying rate.

A parabolic distribution is displayed in the hygroscopic stage. In the capillary zone, we found a different behavior, due to dynamic capillary pressure, since this term depends on the evolution of saturation

$$\left(-\tau \frac{\partial S_w}{\partial t}\right) \quad (36)$$

Fig. 7 shows the mass flux leaving the surface. The pump operates at first to decrease the total pressure, and then a flux of vapor coming from the board increases the chamber pressure. The chamber dynamics are primarily driven by the fluxes leaving the wood, the pump flow rate when switched on, and the eventual rate of condensation on the chamber walls. In practice and for the experimental chamber under consideration herein, the chamber dynamics usually has a time constant much smaller than the internal transfer arising within the wood. The dynamics and the convergence conditions of the wood result mainly from the rapid change of the boundary conditions. Vapor transport is driven by temperature and pump aspiration. We have written the diffusion coefficient as a function that depends on temperature and pressure.

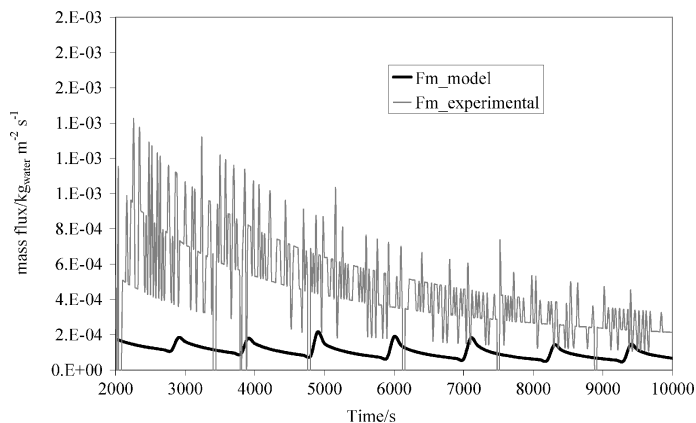


Fig. 7 – Mass fluxes during vacuum drying

A more important pressure is developed by thermal effect, since water vapor depends strongly on temperature (according to gas law). Different values of the coefficient have been proposed in the literature, but it is difficult to have unanimity. In this work, these parameters have been extracted from Hernandez.¹² Fig. 7 reveals passive and active regimes during drying; an acceleration and re-homogenization is visible. The model describes correctly pump action in the wood surface. The pump flux together with the chamber volume defines a

time constant for the pressure evolution when the pump is on (maximum allowable pressure attained), resulting in pressure-decreasing periods. The model can predict some of the more subtle mechanisms observed in practice, such as the increase of mass flux during active regime and moisture distribution in wood and on surface.

Conclusion

We have proposed a numerical solution for a two-scale model for vacuum drying by considering a dynamic capillary pressure, which appears satisfactory. Good agreement between experimental results and those of the simulation is assessed. It is interesting to see how this model allows distinguishing of the phases of vacuum drying, it simulates fast drying phase (active phase) and the stage of homogenization (passive phase).

The coupling between the wood material (product) and dryer (process) is also respected. We have solved a model by considering a dynamic term for capillary pressure. The critical point between capillary and hygroscopic phase is well identified and a drop in moisture content is visualized at the surface. Simulations are relevant because they represent quite well the experimental curves in terms of average kinetic, moisture in the surface, mass fluxes and overall behavior of the dryer by considering a dynamic term that depends on the evolution of saturation.

The simulation is complex because we consider the dryer behavior and wood interaction. The simulation and experimental data are in good agreement, and provide information about the physics of drying. Future research must focus on capillary-hygroscopic transition by considering physical quantities like surface tensions, contact angles between phases, viscosities, pore structure and flow conditions.

ACKNOWLEDGEMENTS

To Instituto Politécnico Nacional (contratación por Excelencia), México and to CONACYT (Repatriación).

Nomenclature

v	– velocity field, m s ⁻¹
k	– permeability, m ⁻²
p	– pressure, mbar
S	– saturation, –
r	– radius of curvature, m
V	– volume, m ³

fsp	– fiber saturation point, –
\bar{V}	– average velocity field, m s^{-1}
K	– phase change rate of water, $\text{kg m}^{-2} \text{s}$
D	– diffusion coefficient, $\text{m}^2 \text{s}^{-1}$
C	– vapor concentration, –
R	– ideal gas constant, $\text{J K}^{-1} \text{mol}^{-1}$
w	– moisture content, kg kg^{-1}
T	– temperature, K
F_m	– mass flux, $\text{kg m}^{-2} \text{s}^{-1}$
aw	– water activity, –
HR	– relative humidity, %
C_p	– specific heat, $\text{J kg}^{-1} \text{K}^{-1}$
t	– time, s
A	– area, m^2
U	– function
h_v	– latent heat of vaporization, kJ kg^{-1}
J	– bound water flux, $\text{kg m}^{-2} \text{s}^{-1}$

Greek letters

μ	– viscosity, $\text{kg s}^{-1} \text{m}^{-1}$
ρ	– density, kg m^{-3}
ϕ	– variable, –
σ	– superficial tension, N m^{-1}
θ	– solvent-particle contact angle, –
ε	– porosity, –
α	– phase, –
λ	– pore size distribution, –
η	– apparent water saturation, –
∇hb	– heat of desorption, J kg^{-1}
λ	– conductivity, $\text{W K}^{-1} \text{m}^{-1}$
Λ	– Lagrangian operator
τ	– damping coefficient
∇	– gradient

Subscripts

i	– specie
c	– capillary
d	– displacement
e	– effective
r	– irreducible water saturation/relative
b	– bound water
g	– gas
l	– liquid
s	– solid

surf	– surface
nw	– non wetting
w	– wetting
v	– vapor
eq	– equivalent
pump	– vacuum pump
cond	– condensate

Superscripts

g	– gas phase
l	– liquid phase
s	– solid phase
dyn	– dynamic
dryer	– dryer
eq	– equilibrium
ch	– chamber
atm	– atmosphere
exp	– experimental
model	– model

References

- Xu, L., Davies, S., Schofield, A. B., Weitz, D. A., *Physical Review Letters* **101** (2008) art. no. 09450.
- Lehmann, P., Assouline, S., Or, D., *Physical Review E* **77**, 056309 (2008).
- Chauvet, F., Duru, P., Geoffroy, S., Prat, M., *Physical Review Letters* **103** (12) (2009).
- Hassanizadeh, S. M., Celia, M. A., Helge, K., *Vadose Zone Journal* **1** (2002) 38.
- Besserer, H., Hilfer, R., Old problems and new solutions for multiphase flow in porous media, In *Porous media: Physics, models, simulation*. Dmitrievsky, A., Panfilov, M. (Eds). World Scientific Publ. Co., Singapore. 2002.
- Van Dijke, M. I. J., Sorbie, K. S., McDougall, S. R., *Advances in Water Resources* **24** (2001) 365.
- Ataie-Ashtiani, B., Majid Hassanizadeh, S., Celia, M. A., *Journal of Contaminant Hydrology* **56** (2002) 175.
- Slattery, J. C., *Am. Inst. Chem. Eng. Journal* **13** (1967) 1066.
- Whitaker, S., *The Method of Volume Averaging. Theory and Applications of Transport in Porous Media*, Kluwer Academic Publishers, Dordrecht, The Netherlands, (1999).
- Perré, P., *Transport in Porous Media* **66** (2007) 59.
- Sandoval, T. S., Marc, F., Jomaa, W., Puiggali, J. R., *Wood Research Journal* **54** (2009) 45.
- J. M. Hernandez, *Séchage du chêne. Caractérisation, séchage convectif et sous vide*. PhD-Thesis Université Bordeaux 1, 1991.
- COMSOL multiphysics©. Version 3.5a.